Medical Engineering & Physics 36 (2014) 786–792

Contents lists available at ScienceDirect

Medical Engineering & Physics

journal homepage: www.elsevier.com/locate/medengphy

Technical note

A low-pass differentiation filter based on the 2nd-order B-spline wavelet for calculating augmentation index

Zijun He[a,b,1], Yongliang Zhang[b,1], Zuchang Ma[b,c,d], Fusong Hu[b], Yining Sun[b,*]

[a] Department of Automation, University of Science and Technology of China, Hefei, Anhui, PR China
[b] Research Center for Information Technology of Sports and Health, Institute of Intelligent and Machines, Chinese Academy of Science, Hefei, Anhui, PR China
[c] Jiangsu Research Institute of Sports Science, Nanjing, PR China
[d] Beijing Sport University, Beijing, PR China

ARTICLE INFO

Article history:
Received 10 July 2013
Received in revised form 6 January 2014
Accepted 8 February 2014

Keywords:
Arterial stiffness
Pulse wave analysis
B-spline wavelets
Convolution
Shoulder point.

ABSTRACT

The key point to calculate augmentation index (AIx) related to cardiovascular diseases is the precise identification of the shoulder point. The commonly used method for extracting the shoulder point is to calculate the fourth derivative of the pulse waveform by numerical differentiation. However, this method has a poor anti-noise capability and is computationally intensive. The aims of this study were to develop a new method based on the 2nd-order B-spline wavelet for calculating AIx, and to compare it with numerical differentiation and Savitzky–Golay digital differentiator (SGDD). All the three methods were applied to pulse waveforms derived from 60 healthy subjects. There was a significantly high correlation between the proposed method and numerical differentiation ($r = 0.998$ for carotid pulses, and $r = 0.997$ for radial pulses), as well as between the proposed method and the SGDD ($r = 0.995$ for carotid pulses, and $r = 0.993$ for radial pulses). In addition, the anti-noise capability of the proposed method was evaluated by adding simulated noise (>10 Hz) on pulse waveforms. The results showed that the proposed method was advantageous in noise tolerance than the other two methods. These findings indicate that the proposed method can quickly and accurately calculate AIx with a good anti-noise capability.

1. Introduction

Augmentation index (AIx) is widely used in assessing arterial stiffness [1,2]. Many clinical researches have proved that the AIx is closely related to cardiovascular diseases [2–4]. Recently, AIx was also used in evaluating the treatments, drug effects, and other related medical researches [5–7]. The key step to calculate AIx is the precise identification of the shoulder point on the waveform. In 1989, Kell et al. first proposed that the shoulder point could be extracted by the fourth derivative of the pulse waveform [8]. And in 1995, Takazawa et al. described the algorithm in detail [9], which has been widely used to calculate AIx [9,10]. As shown in Fig. 1, for type A pulse waveforms, the shoulder point located on the upstroke wave coincides with the first positive-to-negative zero crossing of the fourth derivative; whereas for type C and radial waveforms, the shoulder point located on the downstroke wave corresponds to the second negative-to-positive zero crossing. With diverse positions of shoulder points, the corresponding definitions of AIx are also different (Fig. 1).

Traditionally, the method based on numerical differentiation is used to approximate to the derivate of a signal [11]. However, this method has inherent flaws degrading it in pulse wave analysis (PWA). A major problem is that the numerical differentiation can greatly amplify the noise, especially at high frequencies. Therefore, it is essential to perform appropriate denoising of the pulse wave signal prior to differentiation [12,13]. Unsatisfactorily, it further increases the complexity of the algorithm and may filter out useful information contained in the pulse wave signal [14]. For example, the Savizky–Golay (SG) filters are popularly applied in many fields. When a SG filter is used, high-frequency noise in the pulse wave signal can be largely eliminated by increasing the length or the order of the SG filter. However, some useful details of the signal will be also smoothed out at the same time. In addition, Savitzky–Golay digital differentiator (SGDD), another choice for acquiring the derivative of the pulse wave signal, has the same problem in the choice of lengths and orders [15].

Consequently, it is crucial to develop a new method for calculating the derivative of the pulse waveform, which is able to overcome

* Corresponding author at: Research Center for Information Technology of Sports and Health, Institute of Intelligent and Machines, Chinese Academy of Science, Hefei 230026, Anhui, PR China. Tel.: +86 551 65591104; fax: +86 551 65595621.
E-mail address: ysiim128@aliyun.com (Y. Sun).
[1] These authors contributed equally to this work.

http://dx.doi.org/10.1016/j.medengphy.2014.02.007
1350-4533/

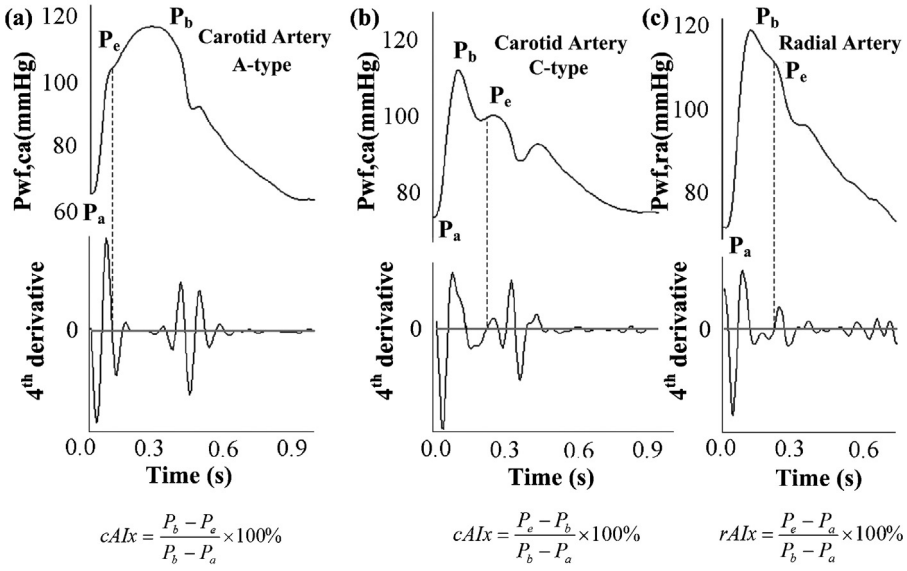

Fig. 1. The relationship between the shoulder point and the 4th derivatives of the pulse waveforms, as well as the corresponding formulae of AIx. (a and b) The types A and C carotid waveforms, while (c) displays a radial waveform.

the aforementioned drawbacks. The differential property of convolution and spline wavelets make it a potential solution. Spline wavelets are widely used in chemistry, image processing and biological signal processing, because they have explicit formulae in both the time and frequency domain [16–18]. In particular, the 2nd-order B-spline wavelet has been used to calculate the high order derivative of chemistry signal successfully [16]. However, the 2nd-order B-spline wavelet has not yet been applied to the calculation of AIx.

The aim of this study is to investigate the accuracy and the anti-noise capability of the proposed method for identifying the shoulder points by the convolution of the pulse wave signal and the function constructed by a cascade of two 2nd-order B-spline wavelets (hereinafter referred to as the convolution method). In the remainder of this paper, we first introduce the principle of the algorithm. Then will be a comparison by form of figure display among AIx calculated by the convolution method, the numerical differentiation and the SGDD for the fourth order differentiation. Subsequently, some waveform examples and a table are given to show the performance of the convolution method on noise tolerance.

2. Theoretical background and algorithm

Wavelets consist of the dilations and translations of a function $\psi(t)$ satisfying a certain condition,

$$\psi_{a,b}(t) = |a|^{-(1/2)}\psi\left(\frac{t-b}{a}\right), \quad a, b \in R; \quad a \neq 0, \tag{1}$$

where a and b are, respectively, the scale and position parameter expressed in real number R. $\psi(t)$ is known as the mother wavelet.

A B-spline wavelet of order m is defined as:

$$\psi_m(t) = 2^{-m+1}\sum_{j=0}^{2m-2}(-1)^j\beta_{2m}(j+1-m)\beta_{2m}^{(m)}(2t-j+m-1) \tag{2}$$

where $\beta_m(x)$ is central B-spline of order m. 2nd-order spline wavelets are used as the tools in this study due to their good performance on calculating the high order derivative of signals [16]. The mother wavelet is defined as

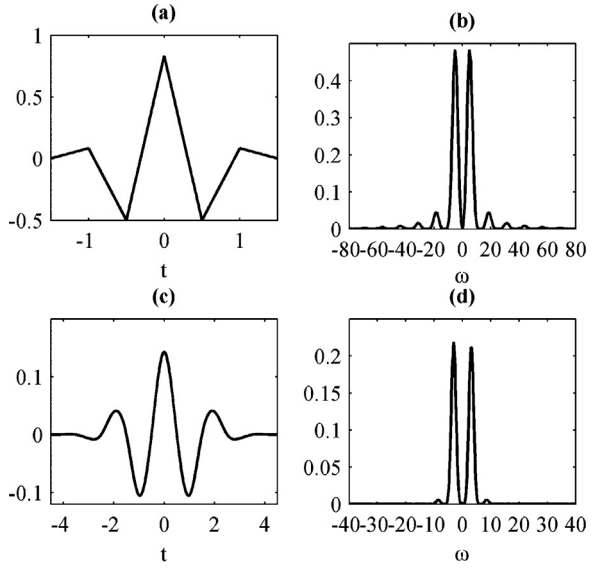

Fig. 2. 2nd-order spline wavelet, function $\varphi_1(t)$ and their Fourier transforms (FT). The 2nd-order spline wavelet (a), FT of the 2nd-order spline wavelet (b), function $\varphi_1(t)$ (c), FT of function $\varphi_1(t)$ (d).

$$\psi_2(t) = \begin{cases} -\frac{1}{6} \times |t| + \frac{1}{4}, & 1 < |t| \le 1.5, \\ -\frac{7}{6} \times |t| - \frac{13}{12}, & 0.5 < |t| \le 1, \\ -\frac{8}{3} \times |t| + \frac{5}{6}, & |t| \le 0.5. \end{cases} \tag{3}$$

$\psi_2(t)$ is an even function and its value is a real number as shown in Fig. 2a. Then we define a new function using $\psi_2(t)$ as:

$$\varphi_a(t) = \psi_{2a}(t) * \psi_{2\times 2a}(t) = |a|^{-(1/2)}\psi_2\left(\frac{t}{a}\right) * |2a|^{-(1/2)}\psi_2\left(\frac{t}{2a}\right) = \varphi_1\left(\frac{t}{a}\right) \tag{4}$$

Obviously, when a is equal to 1, the function $\varphi_a(t)$ is also an even function with a domain of $[-4.5, 4.5]$, which can be see from Fig. 2c. Similarly, we could construct a function refering to Wang [16], and its own fourth derivative is $\varphi_1(t)$. Using Eq. (2), the expression of $\mu(t)$ could be obtained as:

$$\begin{aligned}\mu(t) &= \varphi_1^{(-4)}(t) = \psi_{2\times1}^{(-2)}(t) * \psi_{2\times2}^{(-2)}(t) \\ &= \frac{\sqrt{2}}{288}[\beta_4^{(2)}(2t+1) - 4\beta_4^{(2)}(2t) + \beta_4^{(2)}(2t-1)]^{(-2)} \\ &\quad * [\beta_4^{(2)}(t+1) - 4\beta_4^{(2)}(t) + \beta_4^{(2)}(t-1)]^{(-2)} \\ &= \frac{\sqrt{2}}{18,432}\sum_{n=0}^{10} q_n \cdot \beta_8(2t-5+n) \end{aligned} \quad (5)$$

where $\{q_n\}$ is equal to $[1, 0, -13, -16, 28, 64, 28, -16, -13, 0, 1]$. If $f(t)$ represents a pulse wave signal, the convolution of $f(t)$ and $\varphi_a(t)$ can be written as:

$$\begin{aligned}W(t) &= f(t) * \varphi_a = f(t) * \varphi_1\left(\frac{t}{a}\right) = f(t) * \left[\frac{d^4}{d(t/a)^4}\mu\left(\frac{t}{a}\right)\right] \\ &= |a|^4 \cdot S \cdot \frac{d^4}{dt^4}\left[f(t) * \frac{\mu(t/a)}{S}\right] \end{aligned} \quad (6)$$

where S is the effective area of the function $\mu(t/a)$ defined by

$$S = \int \mu\left(\frac{t}{a}\right) dt \quad (7)$$

The figure of $\mu(t)$ is smooth and similar to a sinc function (as shown in Fig. 3a), and it can be regarded as a low-pass filter according to its Fourier transform (Fig. 3b). So $f(t) * \mu(t/a)/S$ can be taken as the $f(t)$ smoothed by the function $\mu(t/a)$ through convolution. Therefore, we can obtain a smooth convolution signal curve $W(t)$, which is also the dilation of the fourth derivative of pulse wave signal $f(t)$.

Eq. (6) is derived based on the differential property of the convolution of two continuous functions. If the pulse wave signal is sampled every T seconds, Eq. (6) could be written as

$$\begin{aligned}W(t) &= f(t) * \varphi_a(t) \\ &= \int f(\tau) \times \varphi_a(t-\tau)d\tau \approx T \times \sum\nolimits_i f(iT) \cdot \varphi_a[(j-i)T] \end{aligned} \quad (8)$$

where T is the sampling interval, i represents the sample number, and jT is equal to time t. If $\varphi_a(nT)$ is the discrete representation of $\varphi_a(t)$, the discrete Fourier transform of the sequence $\{\varphi_a(nT)\}$ is

$$\begin{aligned}\Phi(e^{j\omega}) &= \sum_{-\infty}^{+\infty}\varphi_a(nT) \cdot e^{-j\omega n} \\ &= \left[\sum_{-1.5a/T}^{1.5a/T}\psi_{2a}(nT) \cdot e^{-j\omega n}\right] \cdot \left[2^{-1/2}\sum_{-3a/T}^{3a/T}\psi_{2\times2a}(nT) \cdot e^{-j\omega n}\right] \end{aligned} \quad (9)$$

It is known that more than 99% of pulse energy concentrates below 10 Hz in healthy persons [21]. By using Matlab, the standardized amplitude-frequency spectrum of $\Phi(e^{j\omega})$ is close to the frequency response of the ideal 4th differentiation filter at low frequencies (as shown in Fig. 3e and f), and the 3 dB cut-off frequency of $\Phi(e^{j\omega})$ is about 9.9 Hz when the scale a is equal to 10/200 and $1/T = 200$. Therefore, the good trade-off between noise-reduction and signal-preservation can be achieved by setting the scale a to 10/200 when the sampling frequency is 200 Hz.

3. Methods

3.1. Subjects

60 healthy adults (30 men and 30 women) aged from 22 to 74 years old (43.5 ± 18.6 years) underwent the measurements of anthropometric parameters. All subjects were free of cardiovascular diseases and vasoactive medications, as assessed by a medical history questionnaire. The study was approved by the local Institutional Review Board.

3.2. Measurements

Before testing, subjects were asked to fast and abstain from cigarettes and alcohol for 3 h or more. After resting in the sitting position for 10 min in a quiet room with a temperature of 20 °C, BP was measured on the left wrist using the oscillometric method (HEM-6000; Omron Healthcare, Kyoto, Japan).

Carotid and radial waveforms were derived using an applanation tonometry-based automated testing device (IIM-2010A; Institute of Intelligent and Machines, Hefei, China). Two arterial applanation tonometers were simultaneously held on the left radial artery and the carotid artery while pressures against the two arteries were obtained and digitized into digital volume pulse using a 12-bit analog-to-digital converter with a sampling frequency of 200 Hz. The pulse wave signals were saved in data files after each measurement.

3.3. Signal processing

3.3.1. Signal pretreatment

We pretreated the wave signals before calculating AIx, respectively, by the numerical differentiation and the reference methods. First, the peaks and troughs of the waveform were identified by searching local maximum and minimum value points of the pulse wave, thus the cycle was determined according to the position of the trough points; then linearity correction of baseline was done sequentially for each cycle of the pulse waveform by the linear equation constructed by the trough points of the current cycle and the next cycle; finally, BP acquired before the test was used to calibrate the amplitude of the pulse waveform.

3.3.2. Calculation of the fourth derivative by the reference methods

Two methods based on the SG algorithm were compared with the convolution method. The former was to calculate the fourth derivative of the pulse wave by the numerical differentiation to acquire AIx values [11]. To acquire a smooth fourth derivative waveform and preserve the waveform, a SG filter by using fitting coefficients of fourth-order polynomials on 35 points, of which the 3 dB cut-off frequency is about 9.9 Hz when the sampling rate is 200 Hz, was used before each differentiation. The latter was the SGDD for the fourth order differentiation by using fitting coefficients of sixth-order polynomials on 35 points [19], of which the 3 dB cut-off frequency is also about 9.9 Hz when the sampling rate is 200 Hz.

3.4. Calculation of AIx

To locate the shoulder point of pulse waveforms, the type of the pulse waveform must be identified first. The method of carotid waveforms classification was assumed by reference to the paper [20]. After obtaining the fourth derivative of the pulse waveform, the shoulder point was determined based on the relationship of the shoulder point and the 4th derivative of the pulse waveform

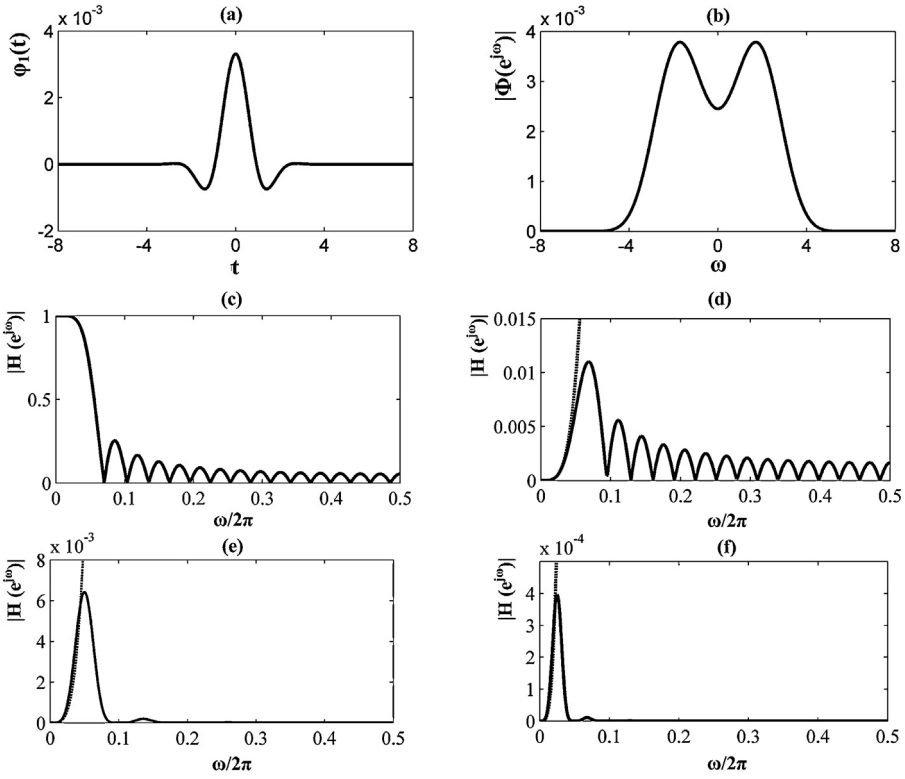

Fig. 3. Function $u(t)$ (a) and its Fourier transform (b), the frequency response of the Savitzky–Golay (SG) smooth filter (c) and one of Savitzky–Golay digital differentiators (SGDDs) for fourth order differentiation (d), as well as the amplitude-frequency spectrum of $\Phi(e^{j\omega})$ when $1/T = 200$ (e) and $1/T = 400$ (f). The dotted line is the frequency response of the ideal 4th order differentiation filter.

(as shown in Fig. 1). The values of AIx at carotid artery and radial artery were calculated by the formulae in Fig. 1.

3.5. Data analysis

To evaluate the consistence of the results, Pearson correlation coefficients and Bland–Altman plots were applied for AIx derived from the convolution method and the other two methods by comparing the averages of AIx of four cycles of the pulse waveforms without added noise. Since the derivative amplifies especially high-frequency noise, and more than 99% of pulse energy is concentrated below 10 Hz in healthy persons [21], we compared the changes of shoulder points identified by the three methods before and after adding high-frequency noise (>10 Hz) on the waveforms.

4. Results

The AIx of carotid pulses and radial pulses evaluated by the numerical differentiation ($cAIx_{Num}$, $rAIx_{Num}$), the SGDD ($cAIx_{SG}$, $rAIx_{SG}$), and the convolution method ($cAIx_{Cov}$, $rAIx_{Cov}$) were compared. Fig. 4 shows the correlation of AIx calculated by the convolution method and the other two methods. The AIx values derived from the convolution methods and the numerical differentiation had a significantly high correlation ($r = 0.998$, $p < 0.001$ for carotid pulses, and $r = 0.997$, $p < 0.001$ for radial pulses), as well as the convolution method and the SGDD ($r = 0.995$, $p < 0.001$ for carotid pulses, and $r = 0.993$, $p < 0.001$ for radial pulses). Moreover, the differences of AIx values calculated by the two methods did not increase with the AIx values as shown in the four Bland–Altman plots (Fig. 4b and d), which satisfied the condition of the analysis of the limits of agreement. The analysis of the limits of agreement for AIx values at carotid artery and radial artery indicated that the mean biases of AIx were close to zero and the values of the standard deviation were not more than 1.8%, which is generally accepted as the evidence of good agreement. These results clearly indicate that the convolution method can accurately calculate AIx.

Fig. 5 displays an example of high-frequency noise effect on the fourth derivative waveforms calculated by the three methods. The fourth derivative waveforms obtained by the three methods were smooth and similar to each other when the pulse waveform was also smooth (Fig. 5a). When high-frequency noise was added to the pulse wave signal, the fourth derivative waveform obtained by the convolution method was still smooth, and the waveform derived by the numerical differentiation was interfered by the noise, while the SGDD yielded worst results. In addition, a statistic result of the mean time changes of shoulder points located by the three methods after adding high-frequency noise was shown in Table 1, from which one could see that the convolution method performed best with the mean time change of 1.4 ± 1.5 ms for carotid pulses, and 1.4 ± 1.3 ms for radial pulses.

5. Discussion

By comparing the values of AIx derived from the three methods, and the anti-noise capability tests, we found that, for the pulse waveforms with high signal-noise-ratio (SNR), the values of AIx derived from the convolution method had high correlations with those derived using the numerical differentiation and the SGDD; for the pulse waveforms with high-frequency noise, we could still get a smooth fourth derivative waveform by the convolution method, and accurately find the shoulder points without any filtering processing. These results indicate that the convolution method can quickly and accurately calculate AIx, and performs well in suppressing the high-frequency noise.

The correlation analysis and Bland–Altman analysis showed good agreement between the convolution method and the other

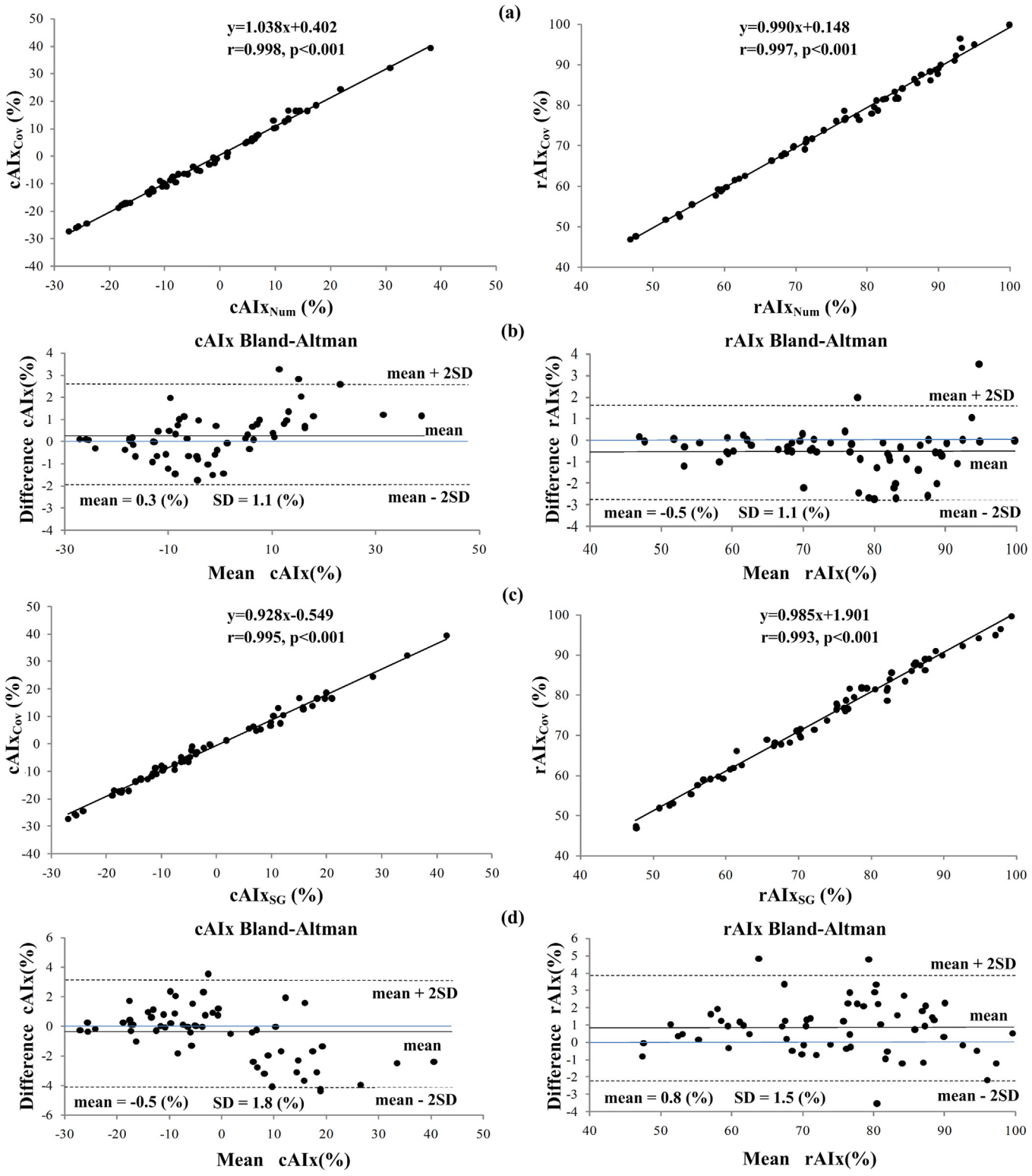

Fig. 4. The correlation of augmentation index (AIx) calculated by the numerical differentiation and the convolution method (a)–(b), as well as the Savitzky–Golay digital differentiator (SGDD) and the convolution method (c)–(d).

two methods (Fig. 4). Convolution calculations play an important role in the field of signal processing due to many significant properties. In this study, the differential property of convolution is well applied to the calculation of the high order derivative of the pulse wave signal.

An ideal full-pass differentiation filter has a gain that increases with frequency (the dotted lines as shown in Fig. 3d–f); therefore, it greatly amplifies high-frequency noise [22]. As shown in Fig. 3, the SG smooth filter, the SGDD and $\varphi_a(t)$ all can be regarded as low-pass filters, of which the 3 dB cut-off frequencies are about

Table 1
The mean time changes of shoulder points determined by the three methods after adding high-frequency noises to the pulse waveforms.

Method	Should points of carotid pulses		Should points of radial pulses	
	Mean (ms)	SD (ms)	Mean (ms)	SD (ms)
The numerical differentiation	3.7	6.5	3.7	4.1
SGDD	36.8	31.2	72.0	35.7
The convolution method	1.4	1.5	1.4	1.3

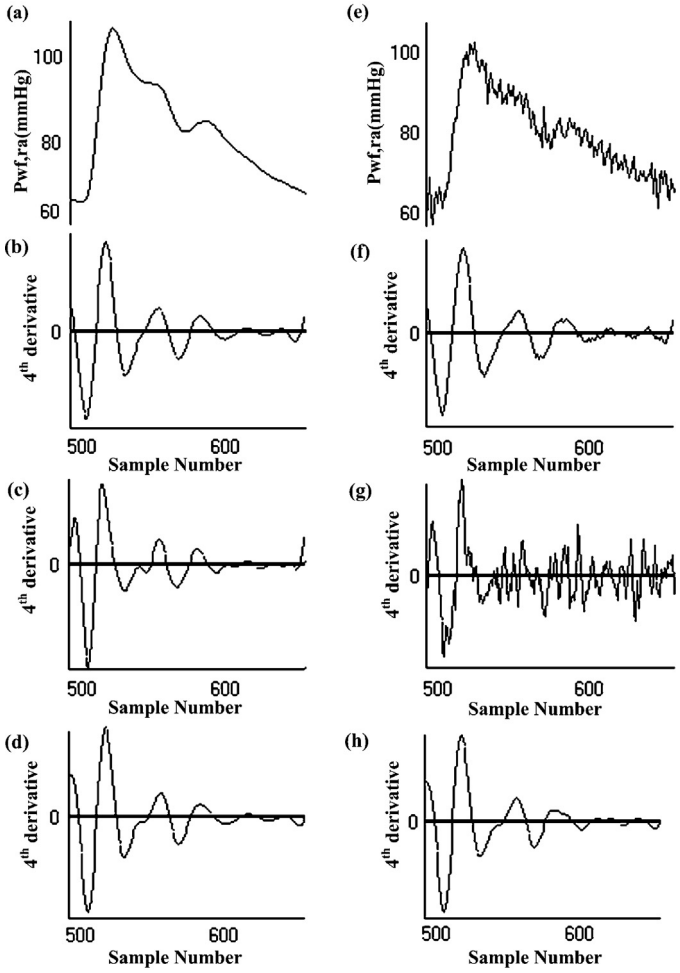

Fig. 5. (a) shows a pulse waveform without added noise and its respective fourth derivative obtained by the numerical differentiation (b), the Savitzky–Golay digital differentiator (SGDD) (c), and the convolution method (d), while (e)–(h) are the corresponding results when the signal-noise-ratio (SNR) is about 29 dB.

9.9 Hz when the sampling rate is 200 Hz; moreover, SG smooth filters and SGDD filters for the fourth order differentiation belong to Type I filters [22,23], of which the frequency responses at $\omega = \pi$ are not zero. However, the amplitude of $|\Phi(e^{j\omega})|$ rapidly decays when ω approaches to zero, and has fewer sidelobes than those of SG smooth filters and SGDD filters. This property enables the convolution method to reduce more high-frequency noise than the other two filters. Because the SG smooth filter is used before each differentiation, the fourth derivative waveform calculated by the numerical differentiation is smoother than that obtained by the SGDD, which actually filters out the noise only once. In addition, increasing the degree of the fitting polynomial or the length of filters may help SG smooth filters and SGDD filters reduce more noise, but this improvement is limited due to the frequency responses of SG smooth filters and SGDD filters.

In our study, The standardized amplitude-frequency spectrum of $\Phi(e^{j\omega})$ is closest to the frequency response of the ideal 4th differentiation filter at low frequency (as shown in Fig. 3) when the scale a is equal to 10/200, and this is independent of sample rate [24], making the convolution method suitable for signals with other sample rates. In contrast, the degree of the fitting polynomial and the length of filters, which are the key parameters of SG smooth filters and SGDD filters, determine the cut-off frequency of filters and need to be properly selected to get a trade-off between noise reduction and signal integrity preservation through many tests [15,25].

Finally, it is important to note that the convolution method described in this study can accurately calculate the fourth derivative of the pulse waveform and locate the shoulder point, without any low-pass filter algorithm even when the pulse signal contains high-frequency noise.

6. Conclusion

In this study, we constructed the function $\varphi_a(t)$ by convoluting two 2nd-order B-spline wavelets, and described a new method by convoluting pulse wave signals with $\varphi_a(t)$, which could accurately calculate the AIx values, and performed well in suppressing the high-frequency noise contained in the pulse wave signal. Our method is able to achieve the effects of filtering and derivations simultaneously, which may have promising beneficial effects in experimental and clinical applications.

Funding

This work was supported by grant 61301059 from National Natural Science Foundation of China, grant 2013BAH14F01 from National Science and Technology Pillar Program and BY2011196 from Jiangsu Province.

Ethical approval

The study was approved by the local Institutional Review Board.

Conflict of interest statement

None declared.

References

[1] Wilkinson IB, MacCallum H, Flint L, Cockcroft JR, Newby DE, Webb DJ. The influence of heart rate on augmentation index and central arterial pressure in humans. J Physiol – London 2000;525:263–70.
[2] Weber T, Auer J, O'Rourke MF, Kvas E, Lassnig E, Berent R, et al. Arterial stiffness, wave reflections, and the risk of coronary artery disease. Circulation 2004;109:184–9.
[3] Cheng K, Cameron JD, Tung M, Mottram PM, Meredith IT, Hope SA. Association of left ventricular motion and central augmentation index in healthy young men. J Hypertens 2012;30:2395–402.
[4] Kingwell BA, Bak C, Gatzka CD. Arterial stiffness and prediction of cardiovascular risk. J Hypertens 2002;20:2337–40.
[5] Liu YP, Thijs L, Kuznetsova T, Gu YM, Asayama K, Stolarz-Skrzypek K, et al. Central systolic augmentation indexes and urinary sodium in a white population. Am J Hypertens 2013;26:95–103.
[6] Nakano T, Munakata A, Shimaura N, Asano K, Ohkuma H. Augmentation index is related to white matter lesions. Hypertens Res 2012;35:729–32.

[7] Janner JH, Godtfredsen NS, Ladelund S, Vestbo J, Prescott E. The association between aortic augmentation index and cardiovascular risk factors in a large unselected population. J Hum Hypertens 2012;26:476–84.
[8] Kelly R, Hayward C, Avolio A, Orourke M. Noninvasive determination of age-related-changes in the human arterial pulse. Circulation 1989;80:1652–9.
[9] Takazawa K, Tanaka N, Takeda K, Kurosu F, Ibukiyama C. Underestimation of vasodilator effects of nitroglycerin by upper-limb blood-pressure. Hypertension 1995;26:520–3.
[10] Hametner B, Wassertheurer S, Kropf J, Mayer C, Holzinger A, Eber B, et al. Wave reflection quantification based on pressure waveforms alone – methods, comparison, and clinical covariates. Comput Methods Programs Biomed 2013;109:250–9.
[11] Friesen GM, Jannett TC, Jadallah MA, Yates SL, Quint SR, Nagle HT. A comparison of the noise sensitivity of 9 QRS detection algorithms. IEEE Trans Biomed Eng 1990;37:85–98.
[12] Madeiro JPV, Cortez PC, Marques JAL, Seisdedos CRV, Sobrinho CRMR. An innovative approach of QRS segmentation based on first-derivative, Hilbert and Wavelet Transforms. Med Eng Phys 2012;34:1236–46.
[13] Georgakis A, Subramaniam SR. Estimation of the second derivative of kinematic impact signals using fractional fourier domain filtering. IEEE Trans Biomed Eng 2009;56:996–1004.
[14] Ciaccio EJ, Micheli-Tzanakou E. Development of gradient descent adaptive algorithms to remove common mode artifact for improvement of cardiovascular signal quality. Ann Biomed Eng 2007;35:1146–55.
[15] Vivo-Truyols G, Schoenmakers PJ. Automatic selection of optimal Savitzky–Golay smoothing. Anal Chem 2006;78:4598–608.
[16] Wang Y, Mo JY, Chen XY. 2nd-order spline wavelet convolution method in resolving chemical overlapped peaks. Sci China Ser B: Chem 2004;47:50–8.
[17] Wang YP, Lee SL, Toraichi K. Multiscale curvature-based shape representation using B-spline wavelets. IEEE Trans Image Process 1999;8:1586–92.
[18] Hsieh CC, Kuo PL. An impulsive noise reduction agent for rigid body motion data using B-spline wavelets. Expert Syst Appl 2008;34:1733–41.
[19] Press WH, Teukolsky S, Vetterling W, Flannery B. Numerical recipes in C: the art of scientific computing. Cambridge, UK: Cambridge University Press; 2002. p. 650–5.
[20] Karamanoglu M. A system for analysis of arterial blood pressure waveforms in humans. Comput Biomed Res 1997;30:244–55.
[21] Wei LY, Chow P. Frequency-distribution of human pulse spectra. IEEE Trans Biomed Eng 1985;32:245–6.
[22] Luo JW, Ying K, Bai J. Savitzky–Golay smoothing and differentiation filter for even number data. Signal Process 2005;85:1429–34.
[23] Oppenheim AV, Schafer RW, Buck JR. Discrete-time signal processing. Upper Saddle River: Prentice Hall; 1999. p. 291–305.
[24] Gans WL, Nahman NS. Continuous and discrete fourier-transforms of steplike waveforms. IEEE Trans Instrum Meas 1982;31:97–101.
[25] Luo JW, Bai J, He P, Ying K. Axial strain calculation using a low-pass digital differentiator in ultrasound elastography. IEEE Trans Ultrason Ferroelectr Freq Control 2004;51:1119–27.